

RESEARCH

Open Access



RC Arch Deck Development and Performance Evaluation for Enhanced Deck Width

Dal-Hun Yang, Min-Jae Kwon, Gi-Ha Eom and Jang-Ho Jay Kim*

Abstract

Due to extreme business competitions in bridge construction industries, the cost reduction became the most important issue in winning a contract bidding. The largest bridge construction cost saving can be obtained by using precasted construction method and by reducing required number of girders, columns, and decks in the bridge system. Therefore, an precasted arch deck system is proposed to widen the lateral span of the deck, which can result in reducing the number of required I-type PSC girders for construction cost saving. A usual lateral width of a flat deck is 1.5–2.0 m, but the width of arch deck is 2.5 m, an increase of 25–60%. Therefore, for a PSC girder bridge with a total width 10 m, a number of required girders needed for ordinary flat RC deck and arch deck is 5 and 4, respectively. This means that one less girder can be required, which means that 20% of girder construction cost can be achieved by using arch deck over ordinary flat deck. In this study, precasted RC arch deck is developed and manufactured to evaluate structural performance of the deck. The study results showed that arch deck has performance exceeding ordinary flat deck and can be used as alternative decks for precasted PSC I-girder bridge construction. The study results are discussed in detail in the paper.

Keywords: RC structures, arch deck, flexural behavior, PSC, I-girder, precasted deck

1 Introduction

Demands for infrastructure have exploded since the early twentieth century as manufactured good transportations exponentially increased. Also, current infrastructure construction trends have focused on reducing construction time by using precasted construction methods to meet large demands of infrastructures and bridge structures by using advanced construction technologies. In recent years, PSC girder bridges are often selected as ridge type for long-span bridge construction for rapid constructions and cost savings (Matta et al. 2006; Kim et al. 1997; Starnas and Whittemore 2005).

Unlike steel bridges where steel cost is expensive, PSC bridges (Han et al. 2003; Jeon et al. 2011; Bhawar et al. 2015) are widely used for their superior economic advantage. PSC bridges are generally constructed using box

girders or I-girders. The box girder (Kim et al. 2008; Cury and Cremona 2010; Kim et al. 2016) has excellent structural advantages such as torsional resistance but its self-weight is relative heavy due to a very large cross-section. Consequently, PSC box girder bridges are constructed for very long span bridges for a span length between 40 and 60 m. In contrast, I-girder (Cho et al. 2013; Han et al. 2010; Jung and Kim 2013) bridges are selected for medium to long span bridges for a span length between 20 and 40 m for economical advantages. In recent years, the introduction of the Incrementally Prestressed Concrete (IPC) method and steel-PSC Hybrid girder (Han and Kim 2001; Kim et al. 2011) improved the load carrying capacity of PSC I-girders, which resulted in increasing the span of the PSC I-girder up to span length of 40–60 m.

However, bridge construction with PSC I-girder requires construction of the decks. Constructing a deck using conventional method of installing formworks and scaffolding at construction site has significant

*Correspondence: jjhkim@yonsei.ac.kr
School of Civil and Environmental Engineering, Yonsei University, 134
Shinchon-dong, Seodaemun-gu, Seoul 03722, South Korea
Journal information: ISSN 1976-0485 / eISSN 2234-13150

shortcomings in terms of constructability and safety. The precast method (Staquet et al. 2004; Shim et al. 2010) was developed to remedy these shortcomings for easy application and improved work safety. The precast methods include development of various types of precast half decks (e.g., LB deck and rib deck) (Lho and Cho 2007; Dey et al. 2013) where the precast half-decks are placed on the girders followed by concrete casting of the rest half of the deck for completion.

Commonly used precast RC decks are manufactured as a flat plate, which supports load only by vertical reaction forces. As a result, they are vulnerable to shear and punching shear failure due to fatigue loading from automobile wheel loading. In contrast, in arch decks, the distributed vertical gravity loading induces compression predominant stresses in the member, which lessens the possibility of cracking. Due to the compression predominant stresses achieved from arching effect (Taylor et al. 2001; Taylor and Mullin 2006; Wu et al. 2006; Marefat et al. 2004; Nam et al. 2009; Jeong and Kim 2014), the arch decks can have longer span and do not fail by tensile cracking. For these advantages, the arch deck can reduce construction cost in PSC I-girder bridge projects.

2 Overview of RC Arch Deck

Arch structures have been applied to numerous constructions from ancient to modern times, due to its structural stability and aesthetic excellence. Due to these advantages, arches have been a cornerstone shape in ancient structures such as stone arch bridges (Heyman 1982) and in constructing cathedral roofs (King 2010; Willis 1848). In recent years, arch have been widely used in machinery, ship, and aeronautical engineering as well as structural and construction engineering such as long span bridge, tunnel lining, etc.

In steel bridge constructions, various types of arch shape steel bridge such as half-tied arch bridge, steel truss arch bridge, concrete filled tube arch bridge, etc. (Nazmy 1997; Cheng 2010; Ma et al. 2011) have been actively developed and constructed. Also, RC and PSC girders which combine economical and mechanical excellence have been studied by applying the structural advantages of arching effect such as RC truss arch bridge, composite girder, double-tied arch bridge, etc. (Tokuno et al. 2005; Won 2013; Kim et al. 2012).

Precast decks used in PSC girders have also been studied extensively. Currently, PSC deck, loop joint deck, Ultra High Performance Concrete (UHPC) deck, etc. (Issa et al. 1995; Ryu et al. 2003; Saleem et al. 2011; Kim and Jeong 2009) have been studied and used in many bridge constructions. Despite the mechanical advantages of arches, there is minute researches on precast decks with arching effect. Therefore, in this study, a precast RC

deck with arch shape is proposed and to evaluate structural performance of the deck by flexural test of single RC arch deck and 2-span composite arch deck.

3 Construction of Experiments of Static Flexural Behaviors

3.1 Specimen Overview

Two types of arch deck specimens were fabricated for static flexural tests: single span specimen (AD) and two-span arch deck composite specimen (BD). BD was fabricated by casting two AD specimens with cast-in-place overlay concrete. The dimensions of the AD were 2500 mm (length) and 1200 mm (width) with 100 mm (midspan cross-section thickness), and 160 mm (end cross-section thickness). As shown in Fig. 2b, it can be seen that there is a slope at the end of the arch deck. It is the location where the cast-in place overlay concrete was filled when assembling two arch decks. The dimension of these slopes are 40 and 80 mm as shown in the figure. Three AD specimens were tested using same conditions. The results of the tested AD specimens are represented by AD 1, AD 2, and AD 3. For BD specimen, only one specimen was manufactured with dimensions of 7200 mm (length) and 2400 mm (width). As shown in Fig. 2b, empty space between the arch decks is the location where the cast-in-place overlay concrete is filled. Including the empty space, a total length is 2400 mm comprised of 1200 mm on two arch decks at left and right side. As stated above, two specimens are placed on RC bed (e.g., representing girders in an actual bridge), which were casted using cast-in-place overlay concrete with 28 days compressive strength of 38.5 MPa. The specimen layout and manufacturing process are shown in Figs. 1, 2 respectively. Especially, the lateral rebars in the AD specimens were connected to the exposed dowel bars in the RC bed using grip coupler as shown in Fig. 2c. The grip coupler works as shown in Fig. 2d, which makes the connection rapid and easy.

3.2 Specimen Fabrication

The specimens used in the static 3-point loading test were fabricated in accordance to the requirements of Korean Highway Bridge Design Code (Limit State Design) (KIBSE 2015). Figure 2 shows the fabrication process. Prior to concrete placement, an arch-shaped steel formwork was manufactured to fabricate AD specimen. After fabricating the formwork, rebars were assembled and concrete was casted. Then, the casted specimen was steam cured to develop sufficient early age strength. After AD specimen was sufficiently cured, connecting AD lateral rebars and reaction force bed rebars were connected using grip couplers. After the rebar connection was completed, a cast-in-place overlay concrete was

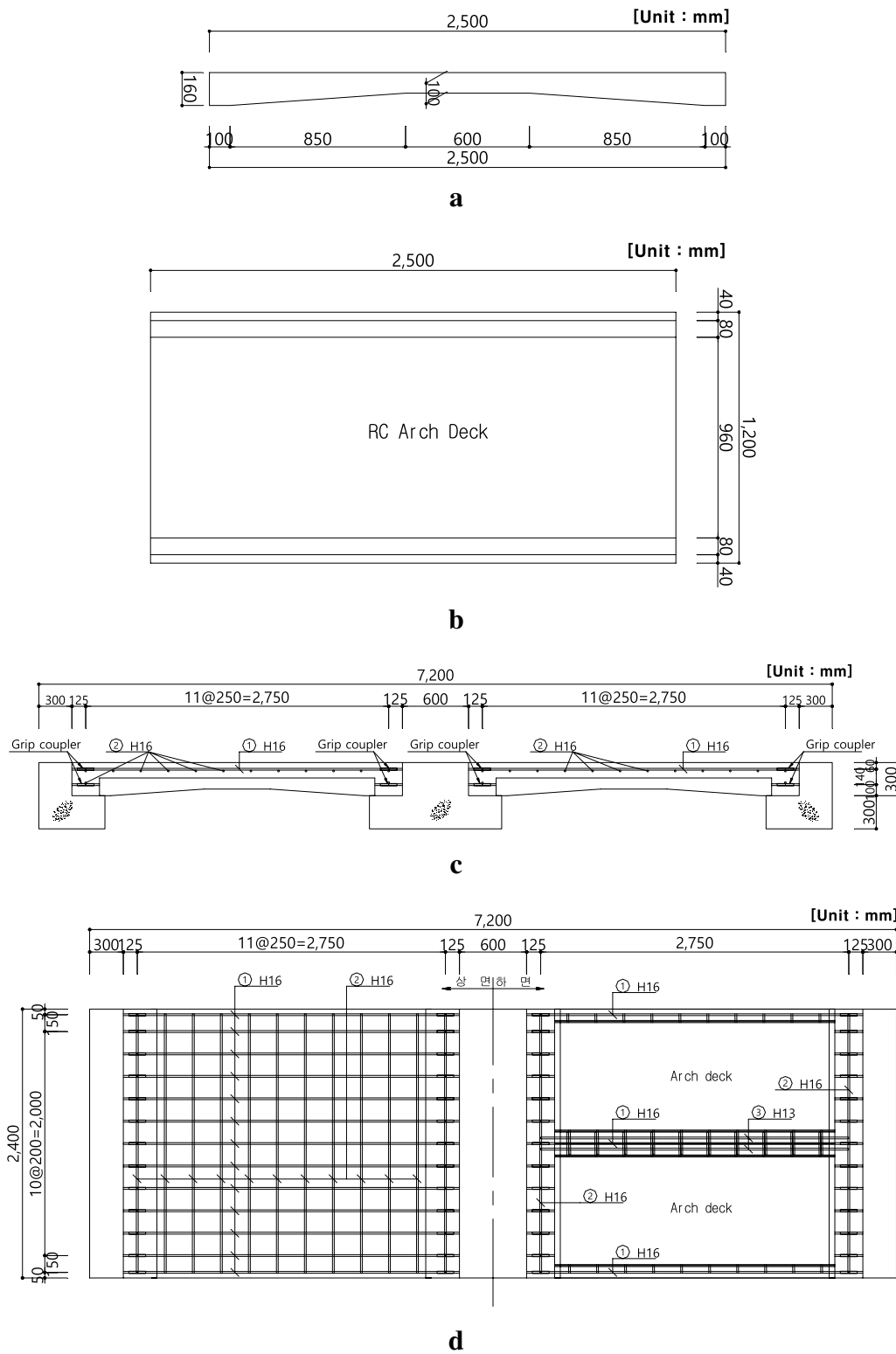


Fig. 1 RC arch deck (AD) and 2-span RC arch deck specimen (BD) layout. **a** Front view of RC arch deck (AD). **b** Top view of RC arch deck (AD). **c** Front view of 2-span RC arch deck specimen (BD). **d** Top view of 2-span RC arch deck specimen (BD).

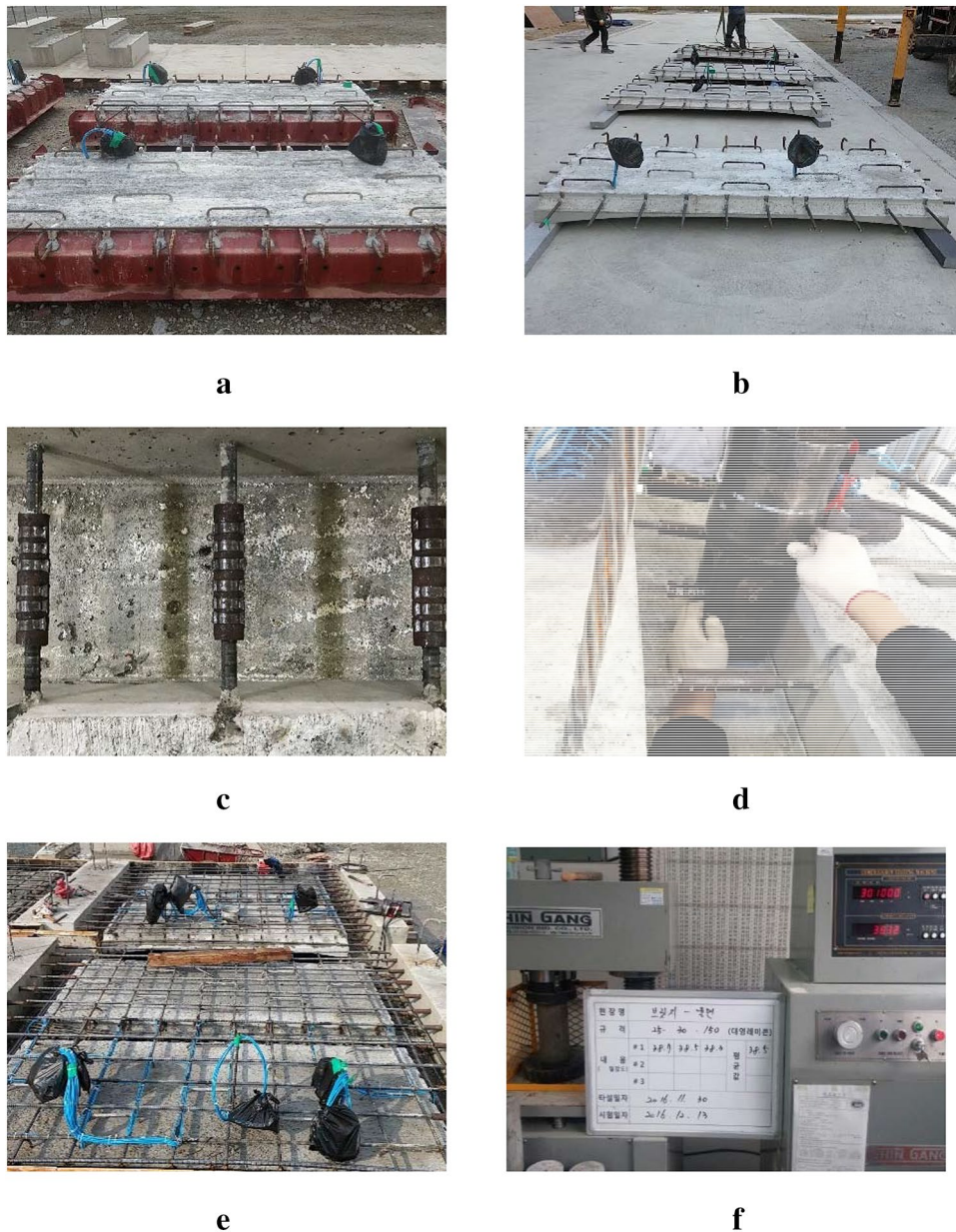


Fig. 2 Manufacture of RC arch deck (AD) and 2-span RC arch deck specimen (BD). **a** Concrete casting and curing. **b** RC arch deck (AD). **c** Grip coupler. **d** Grip coupler setting. **e** Deck and rebar setting. **f** Concrete compressive strength test.

casted, which also was steam cured for development of sufficient early age strength. Figure 2 shows the fabrication process of BD specimen.

The 28 days compressive strength of the concrete of AD specimen and the cast-in-place overlay concrete was set to 40 and 30 MPa, respectively. The compressive strength test results at 28 days revealed that AD specimen and cast-in-place overlay concrete were 49.5 and 38.5 MPa, respectively, both of which exceeded the required design

compressive strengths. The rebars used in the specimens were deformed bars with yield strength of 400 MPa (KSA 2016). The detailed material properties of the specimen are tabulated in Table 1.

3.3 Experimental Method

Two experiments were conducted to represent a vehicle wheel load according to the requirements of Korean

Table 1 Material properties.

Type	Compressive strength of concrete (MPa)		Yield strength of rebar (MPa) (KSA 2016)
	Design value	Test value	
Arch deck (AD1/2/3)	40	49.5	400
Slab	30	38.5	

Highway Bridge Design Code (Limit State Design) (KIBSE 2015) by applying a load using a 230 mm (width) × 580 mm (length) steel plate. The loading area A_p equation is as follows:

$$A_p = \frac{12,500}{9} P (\text{mm}^2) \tag{1}$$

where P is 96 kN, which is 1st class bridge vehicle wheel load requirement in Korea. The ratio of width:length is 1:2.5, and a steel plate with a width of 230 mm and a length of 580 mm.

A quasi-static load was applied to AD specimen using a universal testing machine (UTM) with maximum capacity of 5000 kN. The load sequences followed 3 steps. In step 1, static loading was applied with a loading rate of 1 kN/min within a range of 0–10 kN to obtain the crack load results. The cracks were checked and marked at an interval of every minute, equivalent to a force load of every 2 kN. In step 2, loading was applied with a rate of 2 kN/min within a range of 10–30 kN to verify the structural behavior by loading the specimen after cracking. Cracks were checked and marked as same as in step 1. In step 3, a rate of 0.5 mm/min was applied as a displacement control load from 30 kN on. Cracks were also checked and marked at every 4 min, equivalent to a displacement load of every 2 mm. Static loading was applied when the hydraulic pressure of the loading equipment started to decrease in all experiments, which is an instant just before the specimen reached failure.

Table 2 Static loading test method.

Type	Exp. stage (kN)	Loading rate	Crack checking cycle
RC arch deck (AD)	0–10	1 kN/min	1 min
	10–30	2 kN/min	
	30–P	0.5 mm/min	2 min
2-Span RC arch deck (BD)	0–100	0.3 mm/min	–
	100–500		Per 50 kN
	500–P	0.5 mm/min	Appearance of failure shape

Similarly, a vehicle wheel load was represented as a load to the center of both spans in the quasi-static flexural test of BD specimen. In order to generate the maximum bending moment and to apply exact simultaneous loading to the two spans, a I-shape cross-section steel frame with two rectangular loading plates was used to apply loads on the mid-span of both spans using a static actuator with a maximum capacity of 5000 kN. The loading sequence was divided into two steps. In step 1, a quasi-static load was applied at rate of a 0.3-mm/min as a displacement control mode within a range of 0–500 kN. In step 2, a quasi-static load was applied at a rate of 0.5 mm/min as a displacement control mode within a range of 500 kN to the yield load. Considering safety of the test, the loading was not extended up to the ultimate failure of the specimen. The test results showed that the crack load was identified as approximately 128 kN. Cracks were measured by the naked eye whenever loading was increased from 100 to 500 kN by 50-kN increments.

Table 2 tabulates the loading method and crack measurement time for each step. Figures 3 and 4 show the process of specimen installation and specimen layouts, respectively.

3.4 Overview of Experimental Measurements

The load–deflection relation of the mid-span of the specimen as well as strains of rebar and concrete strain were measured to evaluate the flexural behavior of the specimen. To evaluate the flexural behavior of both AD and BD specimens at various locations, displacements and strains at the 1/4 position (0.25 L), 1/3 position (0.33 L), and 1/2 position (0.5 L) in the lateral direction were measured. A linear variable differential transformer (LVDT) was installed at the bottom surface of AD and BD specimens to measure the vertical displacement. Electric strain gauges of 5 and 60 mm were installed to measure the strain rates of the rebar and concrete, respectively. The cracks formed at the tensile region of AD specimens were visually checked and marked. A Ω-type crack gauge was attached to BD specimen to identify a possible interface opening in the joints in addition to the visual crack

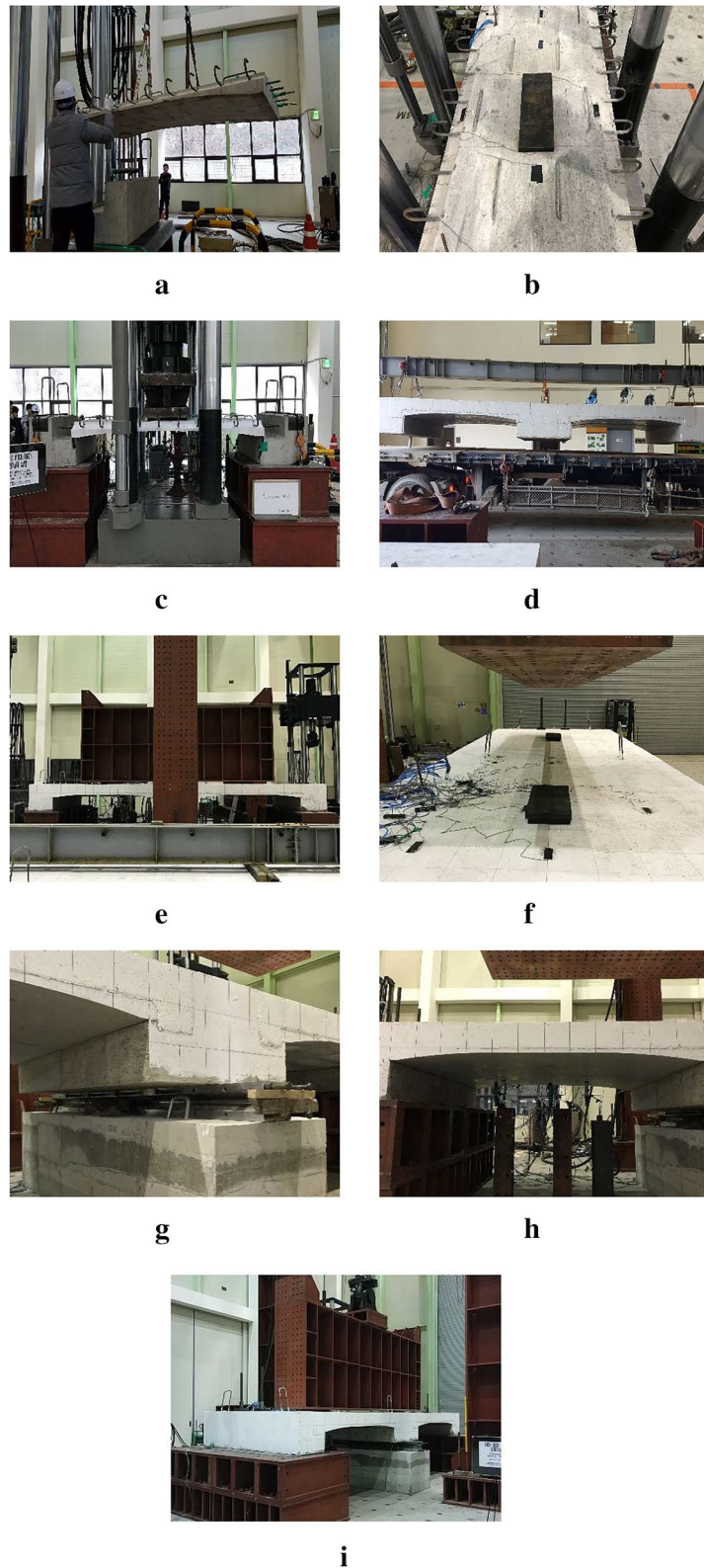


Fig. 3 RC arch deck specimen (BD) static loading test. **a** AD specimen set-up. **b** AD loading area. **c** AD Static loading test. **d** Transporting of specimen (BD). **e** Specimen set up. **f** Static loading area. **g** Hinge detail. **h** LVDT set up. **i** BD Static loading test.

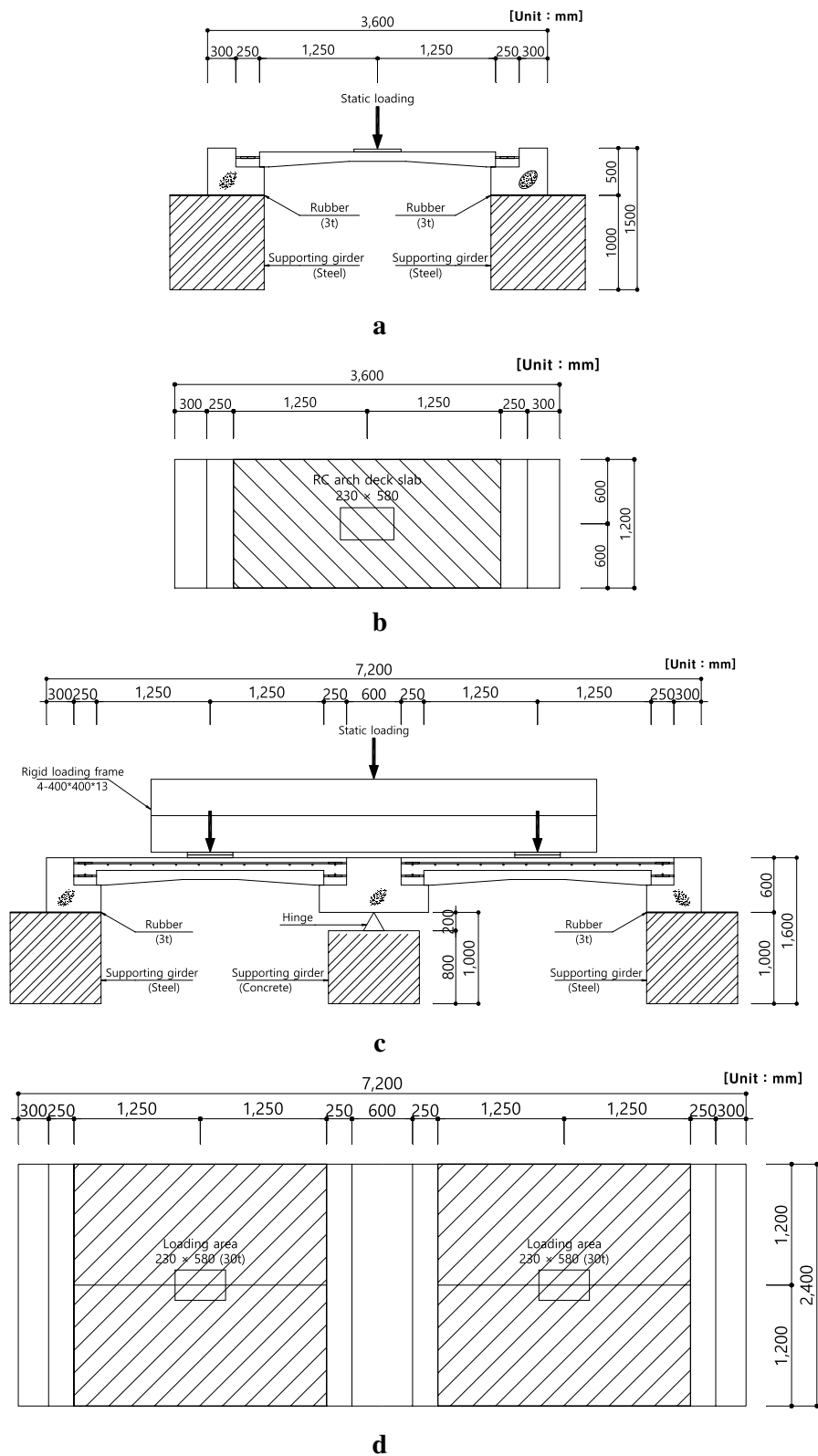


Fig. 4 RC arch deck (AD) and 2-span RC arch deck specimen (BD) static loading test layout. **a** Static loading test cross sectional layout. **b** Static loading test plane layout. **c** Static loading test cross sectional layout. **d** Static loading test plane layout.

checking and marking. The instrumentation layout and setup is shown in Fig. 5.

4 Test Results

4.1 Test Results of AD Loading Test

4.1.1 Load–Displacement Relationship

The design load (P_d), crack load (P_{cr}), ultimate load (P_u), and deflection of the specimen from the design and tests are tabulated in Table 3. The design, crack, and ultimate loads were calculated by the total factored bending moment (M_u) using a combination of dead and live loads, the crack bending moment (M_{cr}) at the transformed section including the rebars, and the nominal bending moment (M_n), respectively, for an assumed span length of 2.4 m.

Load–displacement relation at the center span position of the specimen is shown in Fig. 6. The overall load–displacement relation showed three different slopes, with the first at approximately 0–10 kN range, the second at approximately 10–60 kN range, and the third at approximately 60 kN and later range. The reasons for showing the tri-linear shape of overall structural behavior were due to the following.

The initial slope at the first range (between 0 to 10 kN) was due to a settling of the specimen on the steel frame reaction bed. This settling behavior cannot be interpreted as a structural behavior of AD specimen. Based on the fact that the specimen behaved linearly in the second range (around 10–60 kN), it can be interpreted as elastic structural behavior of the AD after the specimen had completely settled. The displacement of the specimen was then rapidly increased in the third range between approximately 60 kN and on due to concrete cracking and rebar yielding. Since the beginning load of the third range was approximately 60 kN, this is equivalent to approximately 1.6 times the 37.12 kN of design ultimate load (P_w). When applying this design load to the design of an actual structure, the safety factor is approximately 30% higher than the numerical design value.

The maximum static loads of three specimens were 63.20, 61.10, and 69.15 kN, and the mean value was 64.48 kN. This is a level of approximately 1.6–1.9 times the design ultimate load (P_w) 37.12 kN. The summary of the above results demonstrated that the structural performance of AD specimen was sufficiently stable and will have sufficient resistance performance even if cast-in-place concrete is casted on the top of the deck.

The maximum deflection occurred at the center span, and the relationship between load–displacement data by position are shown in Fig. 7 and Table 4. The minimum deflection occurred at the 1/4 position (0.25 L). The deflection at the 1/4 position (0.25 L) was approximately 60–65% of that at the center position (0.5 L). The deflection at the 1/3 position (0.33 L) was approximately 80–85% of that at the center position. The above results verified that the specimen deflected symmetrically with proper distribution of the vertical and horizontal reaction forces.

4.1.2 Load–Strain Relationship

(1) Load–Strain Relation of the Rebar

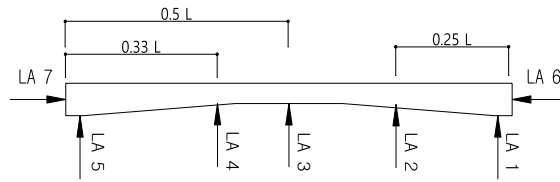
The strain data of the rebar at the 1/4 position (0.25 L), 1/3 position (0.33 L), and center position (0.5 L) of the span in the lateral direction of the specimen are presented in Fig. 8 and Table 5. The strain data showed that the maximum strain occurred at the center position (0.5 L). The measured strains were linearly proportional to the distance difference between the 1/4 and 1/2 positions with the 1/4 position strain being approximately 60–65% of the 1/2 position strain. Also, the strains at the 1/3 position (0.33 L) were approximately 80–85% of those at the 1/2 position.

Since the yield strength of the rebar was 400 MPa, the rebar would yield when the strain rate exceeds approximately 0.002. However, the strain data showed that plastic strain occurred in the rebar at the 1/2 position after a strain of approximately 0.0026. The above results indicate that the yield strain increased due to the arch action from the arch shape of the deck and the coupling effect between rebars and concrete. Due to these reasons, it is considered that strains of rebars, which was embedded in concrete has a slight strain difference than the original rebars. In contrast, the rebar strains at the 1/4 (0.25 L) and 1/3 (0.33 L) positions were approximately 0.002 at the failure loading phase with gradual increasing strains, which showed that rebar yielding did not occur in the rebar at these two positions even at the loading failure phase. The results showed that the load transfer in the specimen occurred as an arch action. Stress and strain relation are shown in Fig. 9a, b, respectively.

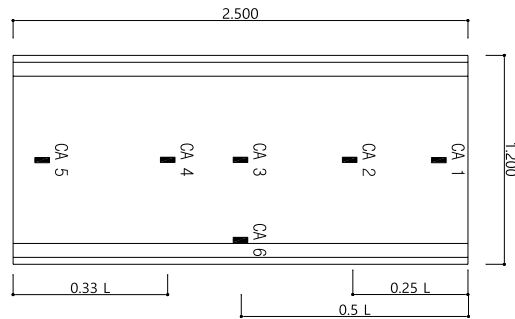
According to the test results, the rebar strain at 1/2 position exceeded the yield strain and reached approximately 0.0035. On the other hand, the rebar strain at 1/3 and 1/4 position stopped at 0.002 level showing that the specimen transferred stresses using arch action.

(See figure on next page.)

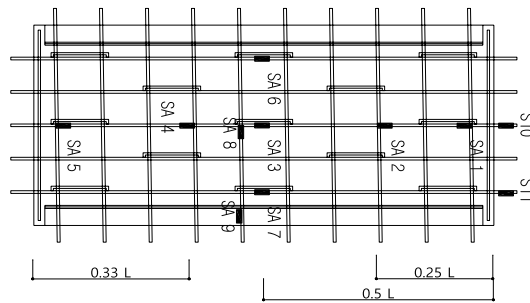
Fig. 5 RC arch deck (AD) and 2-span RC arch deck specimen (BD) sensor locations. **a** AD LVDT locations. **b** AD concrete gauge locations. **c** AD steel strain gauge locations. **d** BD LVDT locations. **e** BD concrete and steel strain gauge and crack gauge locations.



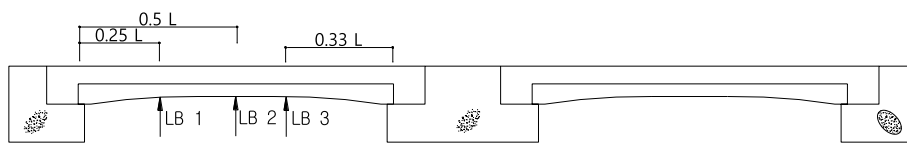
a



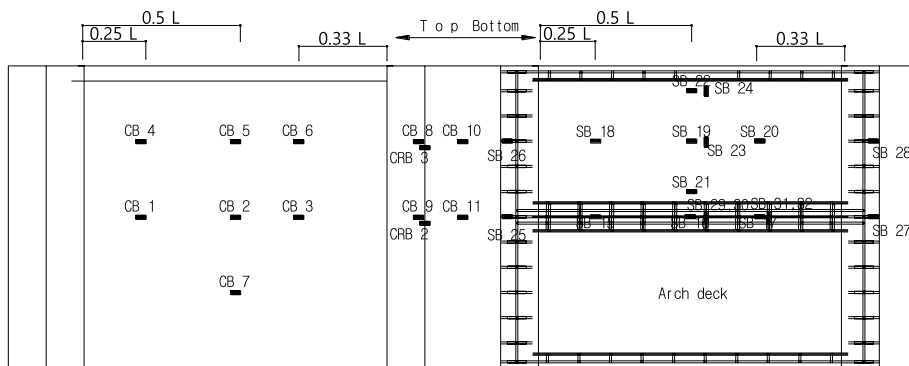
b



c



d



e

Table 3 Design-test data (AD).

Load factor		AD 1	AD 2	AD 3	Average
Design value	P_d (kN)	17.23			
	P_{cr} (kN)	11.71			
	P_u (kN)	37.12			
Test value	P_{cr} (kN)				
	Load (kN)	12.00			
	Disp. (mm)	4.87	4.83	3.45	4.38
	P_d (kN)				
	Load (kN)	63.20	61.10	69.15	64.48
	Disp. (mm)	51.17	62.99	52.49	55.55

Table 4 Test results of load–displacement (AD).

Location	Load (kN)	Displacement (mm)			
		AD 1	AD 2	AD 3	Average
Center point (0.50 L) LA 03	0	0	0	0	0.00
	10	2.19	3.27	2.19	2.55
	30	14.75	18.43	12.97	15.38
1/3 point (0.33 L) LA 04	0	0	0	0	0.00
	10	1.8	2.94	1.77	2.17
	30	13.15	16.26	10.47	13.29
1/4 point (0.25 L) LA 02	0	0	0	0	0.00
	10	1.82	2.16	1.32	1.77
	30	10.05	11.45	7.62	9.71
	60	26.23	34.71	19.27	26.74

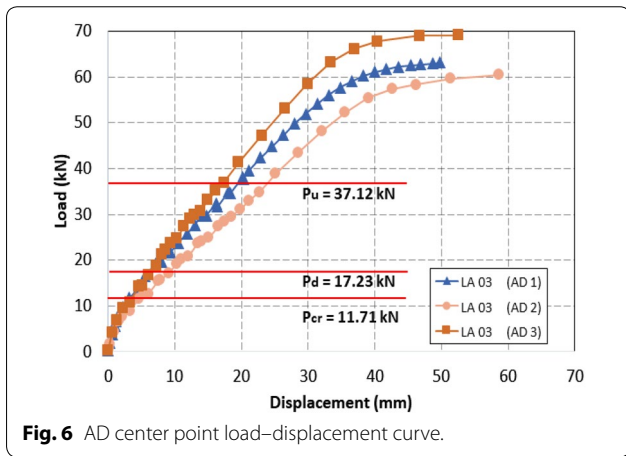


Fig. 6 AD center point load–displacement curve.

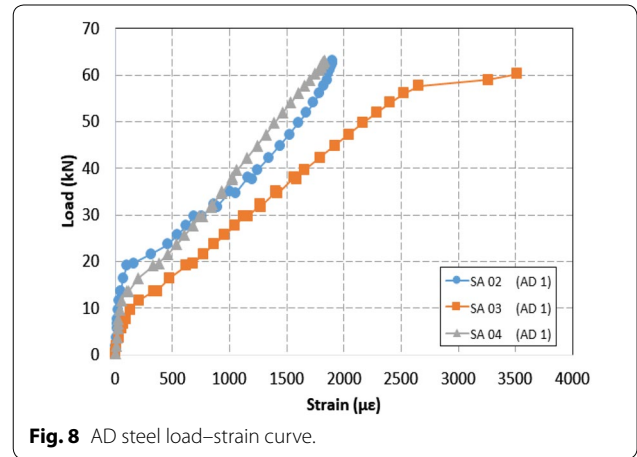


Fig. 8 AD steel load–strain curve.

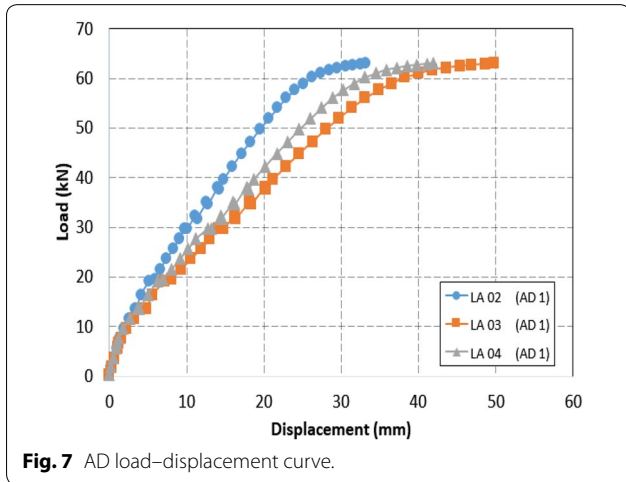


Fig. 7 AD load–displacement curve.

Table 5 Test results of load–steel strain data (AD).

Location	Load (kN)	Strain ($\mu\epsilon$)			
		AD 1	AD 2	AD 3	Average
Center point (0.50 L) SA 03	0	0	0	0	0
	30	1159	1530	1470	1386
	60	3515	4406	2781	3567
1/3 point (0.33 L) SA 04	0	0	0	0	0
	30	761	1321	986	1023
	60	1748	3070	2356	2391
1/4 point (0.25 L) SA 02	0	0	0	0	0
	30	755	611	130	499
	60	1864	1846	1338	1683

(2) Load–Strain Relation of the Concrete

Strain curve and data of the concrete at the 1/4 position (0.25 L), 1/3 position (0.33 L), and center position (0.5 L)

of the arch deck in the lateral direction of the specimen are presented in Fig. 10 and Table 6. The concrete strain did not have the same level of strain results as 60–65 and

80–85% at the 1/4 and 1/3 position, respectively, shown in the rebar. The reason for this was due to cracking concrete material characteristic, compared to continuous and uniform straining characteristic of rebar.

The load–strain relation of concrete showed a similar behavior at the center position to that of rebar. However, at the 1/4 position, a second slope change was observed at approximately 30 kN, which is equivalent to a strain of approximately 27% of the yield strain occurring at the center position. The delayed strain occurrence at the 1/4 position compared to the center showed that the arch action has occurred.

The overall curve shape and slope change at the center position of the rebar and concrete were similar in all 3 specimens without significant errors in the measurements.

In addition, the load reached a failure load of approximately 60 kN, while the strain did not reach a concrete compressive strain limit of 0.003. This result indicated that compressive region of the specimens may have structural resistance even at ultimate load from the experiment of 60 kN.

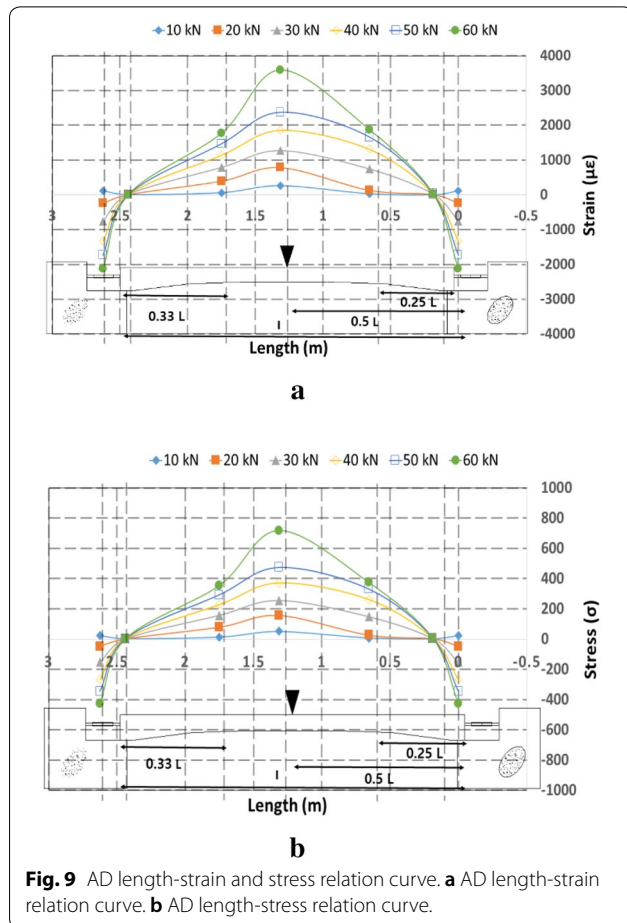


Fig. 9 AD length-strain and stress relation curve. **a** AD length-strain relation curve. **b** AD length-stress relation curve.

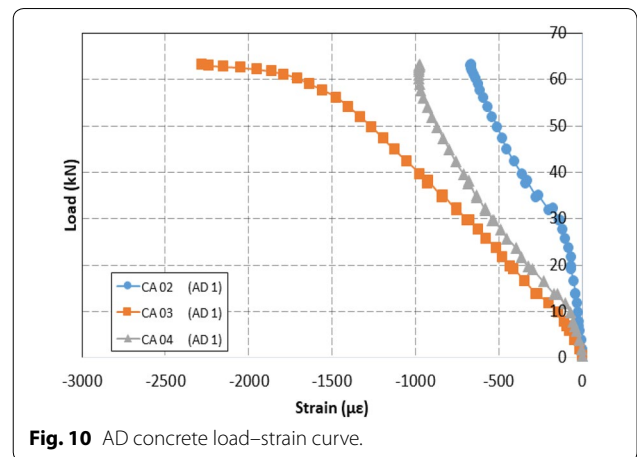


Fig. 10 AD concrete load–strain curve.

Table 6 Test results of load–concrete strain data (AD).

Location	Load (kN)	Strain (µε)			
		AD 1	AD 2	AD 3	Average
Center point (0.50 L)	0	0	0	0	0
CA 03	30	−693	−1085	−923	−900
	60	−1710	−2679	−1707	−2032
1/3 point (0.33 L)	0	0	0	0	0
CA 04	30	−540	−744	−602	−629
	60	−981	−1200	−1239	−1140
1/4 point (0.25 L)	0	0	0	0	0
CA 02	30	−141	−437	−288	−289
	60	−642	−1018	−781	−814

4.1.3 Crack Shape

All specimens showed longitudinal crack pattern from flexural failure. As mentioned previously, the cracks were checked and marked at every 2 kN of applied loading. No cracks were found until 12 kN. This crack result is similar to the design crack load of 11.71 kN. After the initial cracking, multiple cracks formed and propagated during applied loading range of 12–30 kN as the width of the existing cracks tended to increase rather than generating new cracks. After 30 kN of loadings, which indicates that tensile failure occurred at the bottom surface of the specimen, at which point the load was only resisted by rebars.

The overall crack pattern of a longitudinal macro-cracks was observed at the center of the specimen. However, no longitudinal and lateral cracks were observed beyond the 1/4 position, which once again shows that arch action occurred in the load transferring process where the macro-cracking occurred at the weakest location, the top of arch in the specimen. The crack shape of AD specimen is shown in Fig. 11.

4.2 Test Results of BD Loading Test

4.2.1 Load–Displacement Relationship

The comparison of load–displacement relation with the crack load (P_{cr}), design load (P_d), and ultimate load (P_u) is shown in Fig. 12. The overall linear behavior is shown prior to the design load (P_d) of approximately 306.45 kN. However, the load–displacement relation showed nonlinear behavior after the design load due to rapid increase in strains, which comes from stiffness reduction due to concrete cracking beyond the design load. The comparison of design and test load data is presented in Table 7.

The failure load of the BD was 922.80 kN, which is approximately 2.4 times the design ultimate load (P_u) of 384.31 kN, showing that the load carrying capacity of the arch deck was much higher than that of the design values obtained using a flat deck. In AD arch deck test results, the maximum failure load occurred at approximately 1.75 times the average design ultimate load. In BD arch deck test, the failure load occurred at approximately 2.4 times the design load due to better composite behavior between AD single deck and cast-in-place fill in overlay concrete. BD specimen test results are more realistic indication of the performance of the arch deck since it shows from the composite behaviors of 2 span decks with deck-overlay concrete system. Since, the failure load of the arch deck

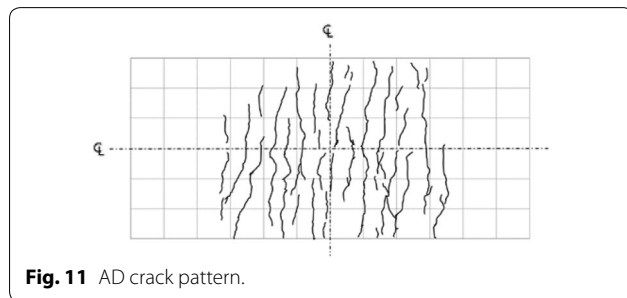


Fig. 11 AD crack pattern.

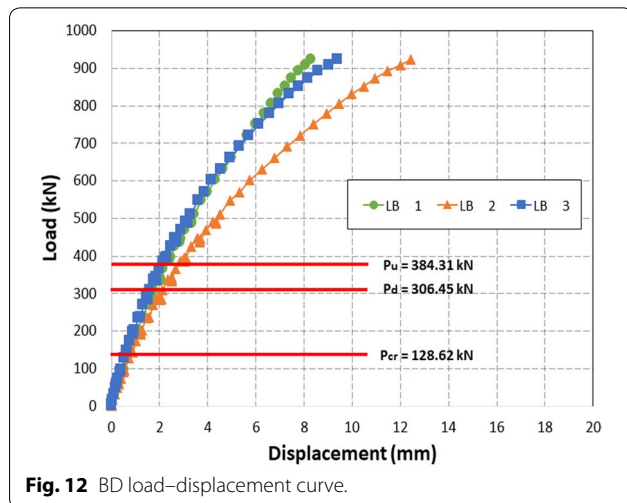


Fig. 12 BD load–displacement curve.

Table 7 Comparison of design-test data (BD).

Index	P_{cr} (kN)	P_d (kN)	P_u (kN)
Design value	128.62	306.45	384.31
Test value	250.00	–	922.80

is approximately 30–40% flat deck, greater than that of an ordinary the reduction of deck thickness and rebar usage can be implemented in the design of the arch deck to lower construction costs and improve constructability.

The comparison of displacements at the 1/4 position (0.25 L), 1/3 position (0.33 L), and 1/2 position (0.5 L) in the lateral direction of the first span of the BD with the design values are summarized in Table 8. The maximum deflection of the specimen was found to be 12.41 mm at the 1/2 position (0.5 L). The deflections at the 1/4 and 1/3 positions were approximately 65 and 75% of that at the 1/2 position, respectively. Also, the results showed that there was no torsional problem in the arch deck based on uniform crack pattern and stable failure mode, showing uniform load distribution to both spans.

4.2.2 Load–Strain Relationship

(1) Load–Strain Relation of the Rebar

The load–strain relations of the rebar at the 1/4, 1/3, and 1/2 positions from the first span of BD specimen and AD specimens in the lateral direction are shown in Fig. 13. The maximum strain of the rebar was approximately 0.0034, occurring at the 1/2 position (0.5 L) under the maximum load of 922.80 kN. However, plastic strain was observed in the rebar at strain of approximately 0.0025 before the maximum strain was measured, indicating rapid strain increase after yielding.

Since the yield strength of rebar used in this specimen was 400 MPa, its yield strain was approximately 0.002. However, as analyzed in previous studies, plastic strain of the rebar actually occurred after total strain of approximately 0.0026, which is the same strain behavior shown in the AD test. For the above reason, the rebar yielded at approximately 900 kN and a total strain of 0.0026 rather than at approximately 750 kN and a total strain of 0.002 of the design value. Furthermore, a slope change was observed at a load of approximately 300 kN, which was equivalent the design load (P_d) of 306.45 kN.

Also, at the 1/4 and 1/3 positions, a slope change occurred at a load of approximately 600–700 kN. Even though the ultimate load was reached, the maximum strain did not reach a yield strain of 0.002. Based on the above results, there exists structural resistance remaining 1/4 and 1/3 positions may have structural resistance.

Table 8 Test results of load–displacement (BD).

Location	Load (kN)	Displacement (mm)		
		1/4 point (0.25 L) LB 1	1/2 point (0.5 L) LB 2	1/3 point (0.33 L) LB 3
RC arch deck specimen (BD)	0	0	0	0
	300	1.76	2.13	1.61
	400	2.47	3.01	2.30
	500	3.44	4.49	3.28
	600	4.30	5.74	4.16
	700	5.31	7.29	5.31
	800	6.64	9.46	6.97
	900	8.07	11.99	8.58
	922.80	8.30	12.41	9.39

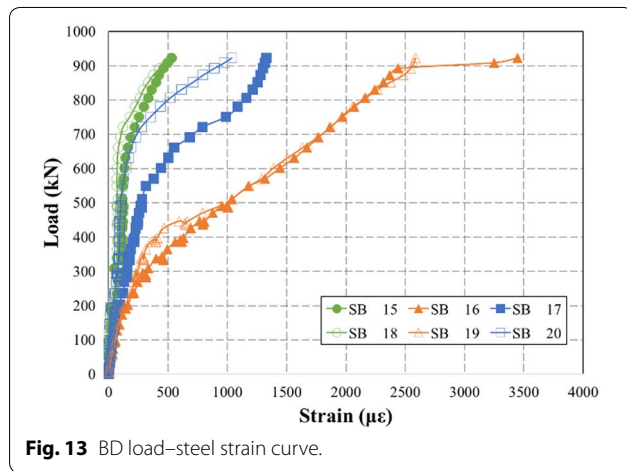


Fig. 13 BD load–steel strain curve.

Since tensile strain was observed in the rebars in the test, the neutral axis of the arch deck was located above the bottom rebars. Similar to AD specimens, due to the relatively small height of the arch compared to its width,

the bottom rebars resisted the tensile strain occurring at the lower region of the specimen. The strain data of the rebar at the 1/4 and 1/3, and 1/2 positions of the first span in the lateral direction of the specimen are tabulated in Table 9. This strain data showed that the 1/2 position reached the theoretical yielding strain of 0.002 at approximately 800 kN. Then after a load of 900 kN, the strain increased sharply, confirming that the steel actually yielded.

(2) Load–Strain Relation of the Concrete

The load–concrete strain relation at the 1/4, 1/3, and 1/2 positions of the fill-in overlay concrete in the specimen is shown in Fig. 14. As shown in the Fig. 14 the maximum strain occurred at the 1/2 position and was approximately 0.0017, which is less than the ultimate concrete compressive strain of 0.003. A compressive failure did not occur in the specimen even at the ultimate load of 922.80 kN, showing that the arch deck has sufficient resistance against brittle compressive failure.

Table 9 Test results of load–steel strain data (BD).

Location	Load (kN)	Strain (ε)		
		1/4 point (0.25 L) SB 15	1/2 point (0.5 L) SB 16	1/3 point (0.33 L) SB 17
RC arch deck specimen (BD)	0	0	0	0
	300	46	335	157
	400	114	628	218
	500	124	1000	277
	600	133	1445	442
	700	188	1770	683
	800	333	2160	1159
	900	463	2438	1302
	922.80	531	3445	1329

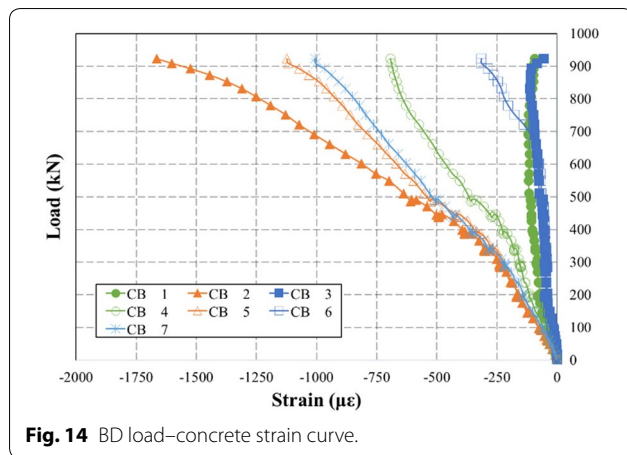


Fig. 14 BD load–concrete strain curve.

Furthermore, the maximum strains of CB 5 and CB 7 attached at the 1/4 position (0.25 L) were approximately 0.001, which has no effect on failure of the deck.

In contrast, it was found that the strains of CB 1 and 3 and CB 4 and 6 attached to the 1/4 and 1/3 positions were minimal, showing the load transfer in the arch deck was effective due to arch action.

The strain data at the center of the longitudinal direction and the 1/4, 1/3, and 1/2 positions of the specimen are tabulated in Table 10. This strain data show that the strains of all positions strain did not reach the strain limit of concrete compressive failure.

4.2.3 Crack Shape and Data

The crack pattern of the tested specimen is shown in Fig. 15. Since two AD were combined, each of the AD was separately denoted. The cracks were checked and marked from a load of 100 kN at every 50 kN increment. The initial crack occurred at a load of approximately 250 kN. Since the design crack load (P_{cr}) was 128.62 kN, the

actual crack load was approximately 1.9 times the design crack load, which verifies effective load transfer in the structure due to arch action. The visible crack propagation started at a load of approximately 600 kN. The longitudinal crack was observed up to a load of approximately 600 kN, but the radial crack was also partially observed along with the crack in the longitudinal direction from a load of approximately 700 kN. There are two reasons for the cracking behavior. ① Since the loading steel plate was arranged in the transverse direction, loading was distributed in the longitudinal direction as well as in the transverse direction. ② The ratio of lengths in the longitudinal and transverse directions was nearly 1:1 in the span. Based on the reported study results on punching shear by Choi et al. (2017), radial cracks occur when the ratio of cross-sections is 1:1. It is important to note that, since the BD had no reaction bed in the longitudinal end and transverse stiffness was stronger, most cracks were in longitudinal direction. From a load of approximately 800 kN, existing longitudinal cracks propagated and new longitudinal cracks formed rather new radial cracks. In the maximum load, longitudinal cracks were advanced further, it was predominantly comprised of longitudinal cracks from the effect of flexural failure mode.

A crack gauge of CRB 1 was attached to check the cracking or separation at the AD joint to fill-in overlay concrete. Also, crack gauges CRB 2 and CRB 3 were attached to check cracking and gap opening between the overlay concrete and reaction bed. Strain data are shown in Fig. 16. In CRB 1, the gap separation opening at the AD joints progressed rapidly at a load of approximately 300 kN as overall displacement and strain increased. This is an inevitable result when using the precasted deck construction, resulting in formation of multiple cracks. Also, since this joint cracking load was approximately 2.33 times higher than the design crack load (P_{cr}) of 128.62 kN, it is possible to disregard

Table 10 Test results of load–concrete strain data (BD).

Location	Load (kN)	Strain (ε)		
		1/4 point (0.25 L) CB 1	1/2 point (0.5 L) CB 2	1/3 point (0.33 L) CB 3
RC arch deck specimen (BD)	0	0	0	0
	300	−82	−250	−46
	400	−103	−395	−55
	500	−109	−605	−62
	600	−115	−813	−79
	700	−121	−1011	−92
	800	−109	−1251	−110
	900	−96	−1525	−106
	922.80	−93	−1664	−55

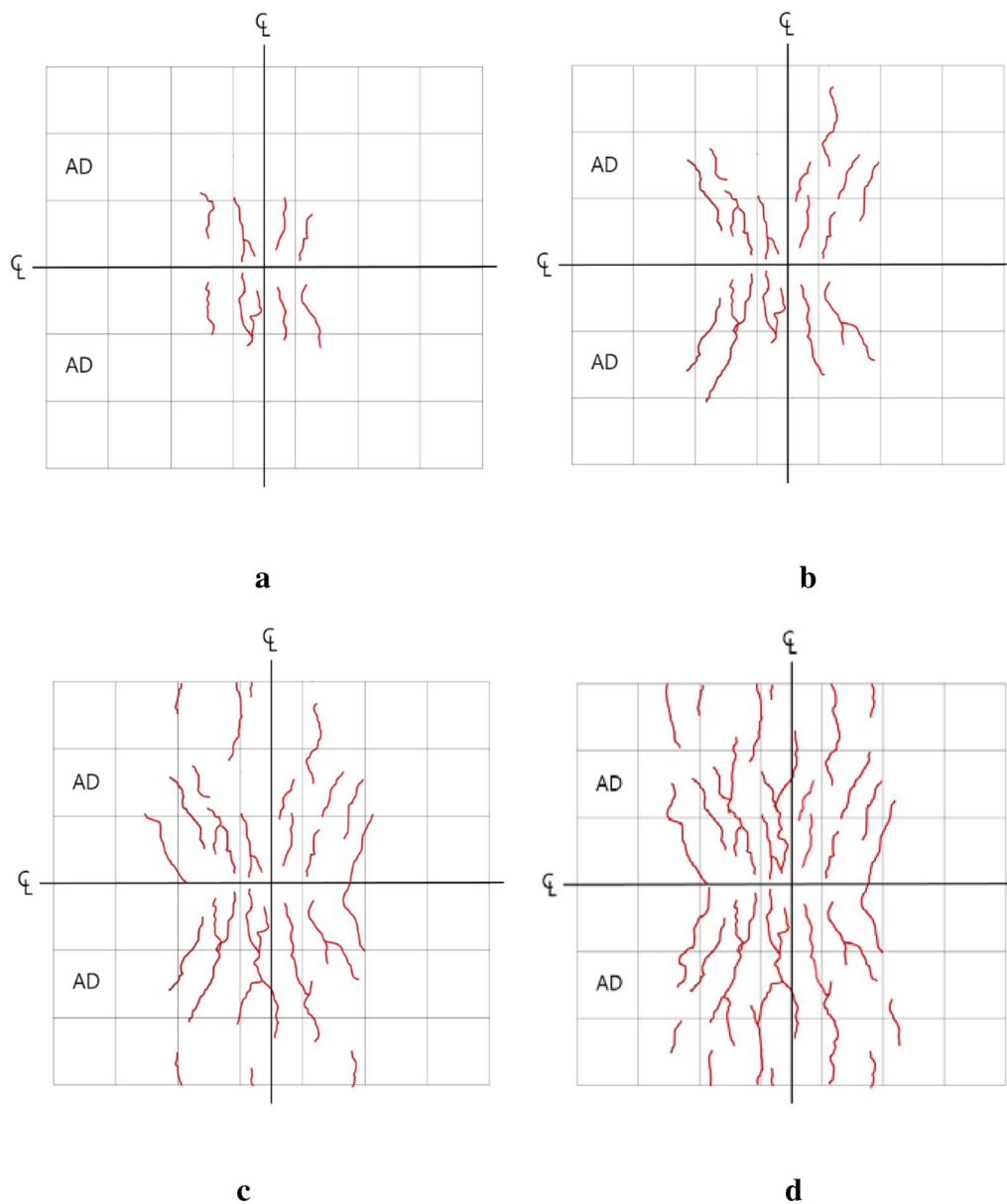


Fig. 15 BD crack pattern. **a** 600 kN. **b** 700 kN. **c** 800 kN. **d** 922.80 kN.

the cracks and considered to be insignificant defect in structural performance. In contrast, the cracks in fill-in overlay concrete and reaction bed had similar cracking behavior where the cracks propagated up to a load of approximately 900 kN with a behavior different than those of CRB 1. From the crack pattern, it is safe to conclude that the crack phenomenon in the fill-in overlay concrete and reaction bed showed stable failure behavior even at the ultimate design load (P_u).

5 Analysis Results

In this study, finite element analysis (FEA) was performed to predict and verify the experimental results. MIDAS FEA was used for the simulation, which was conducted by applying the same boundary conditions and material properties as those used in the experiment.

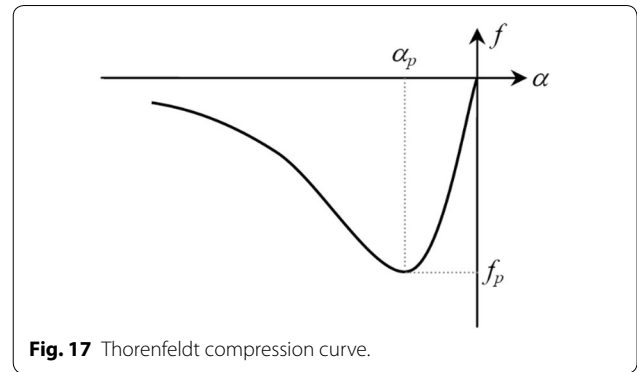
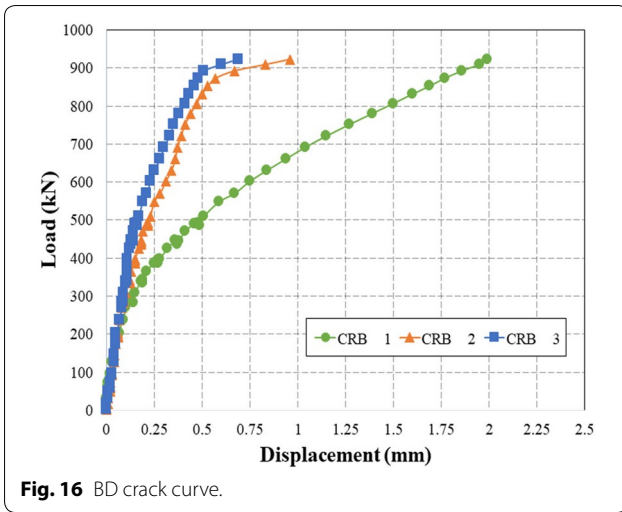


Fig. 17 Thorenfeldt compression curve.

5.1 Rebar and Concrete Model

In this study, concrete and rebar were modeled using hexahedral and bar solid element, respectively.

For concrete, a total strain crack model and the discrete crack model were used. According to a method that handles a crack axis, two methods (fixed and rotating crack models) are provided. The fixed crack model assumes that once a crack axis is determined, it does not change. The rotating crack model assumes that the crack direction rotates continuously according to the change in principal strain. The fixed crack model can represent physical characteristics about crack phenomena in detail, whereas the orthogonal crack model tends to overestimate stiffness and strength slightly compared to that of the non-orthogonal crack model. In contrast, the rotating crack model does not need to remember previous crack states; its algorithm is relatively simple, resulting in superior convergence. Due to this advantage, the rotating crack model has been employed for a long period of time as a non-linear analysis method for reinforced concrete structures.

The compressive model in the total strain crack model used in this study is shown in Fig. 17. This study employed Thorenfeldt hardening curve, which was a hardening–softening curve given as follows:

$$f = -f_p \frac{\alpha_i}{\alpha_p} \left(\frac{n}{n - 1 + \left(\frac{\alpha_i}{\alpha_p}\right)^{nk}} \right) \tag{2}$$

where, $n = 0.80 + \frac{f_{cc}}{17}$ and $k = 1$ when $0 > \alpha > \alpha_p$ and $k = 0.67 + \frac{f_{cc}}{62}$ when $\alpha \leq \alpha_p$.

The tensile model is shown in Fig. 18. It used Hordijk curve (Hordijk 1991), which is a model that generates softening if the tensile strength is exceeded.

For the failure criteria of rebar, von Mises failure criterion was applied to conduct the analysis.

5.2 Specimen Modeling

The material properties used in the analysis are tabulated in Table 11. For the boundary conditions, fixed end and center hinges were used to represent the experimental condition as shown in Fig. 3 and 4, respectively.

5.3 Analysis Results of AD Test

The contour and crack pattern obtained from the finite element analysis results are shown in Fig. 19. The overall stress distribution showed longitudinal crack pattern from flexural failure. The load–displacement relation comparison between the experiment and analysis results at the 1/2 position is shown in Fig. 20. MIDAS FEA was used for the simulation, which was conducted by applying the same boundary conditions and material properties as those used in the experiment. The analysis results verified that the initial slope of the load–displacement curve changed at a load of approximately 10 kN, as same as in the test result. The structural behavior of AD test simulation included the arch deck connected to the

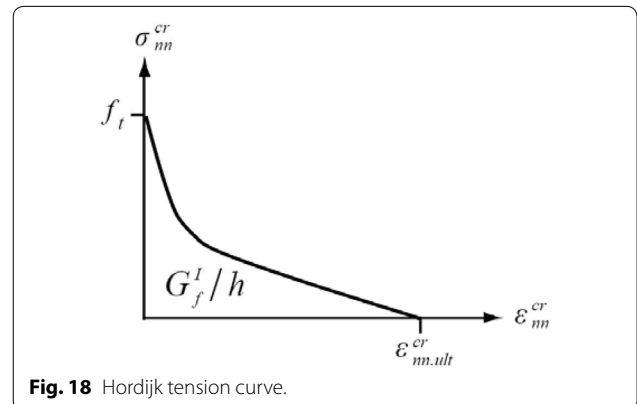


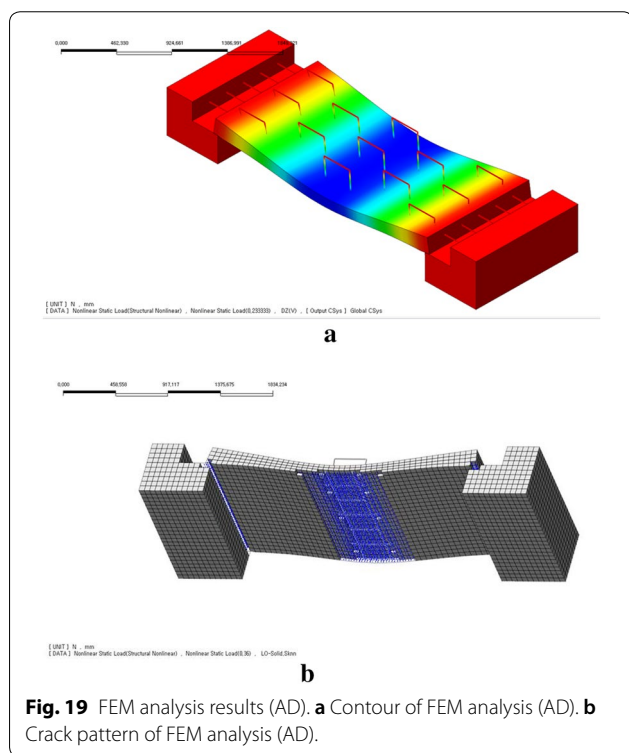
Fig. 18 Hordijk tension curve.

Table 11 Analysis material properties.

Index	Concrete		Rebar
Material	OPC		SD400
Strength (MPa)	Arch deck	$f_{ck} = 50$	$f_{ck} = 400$
	Overlay concrete	$f_{ck} = 40$	
Elastic modulus (N/mm ²)	Arch deck	28,628	203,000
	Overlay concrete	31,099	
Poisson's ratio	Arch deck	0.167	0.3
	Overlay concrete	0.167	
Weight density (N/mm ²)	Arch deck	2.3×10^{-5}	7.9×10^{-5}
	Overlay concrete	2.3×10^{-5}	

reaction bed by rebars, in which both contributed to the composite structural behavior.

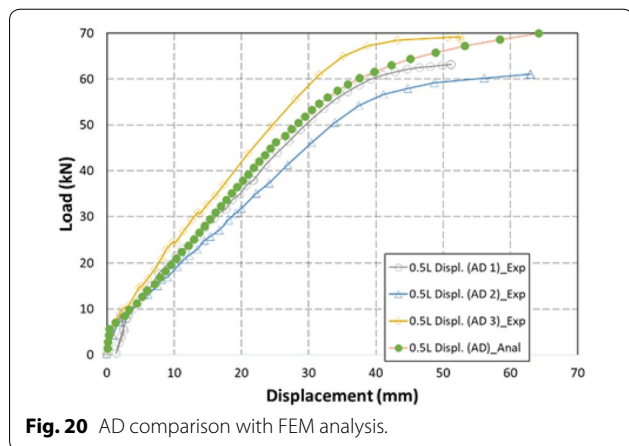
In the simulation, the deflection of AD increased rapidly starting from a load of approximately 60 kN, which indicates that the structural resistance of the AD reached its limit when a load of approximately 60 kN is applied. More specifically, starting from a load of 60 kN, the numerical simulation showed that the AD had ductile deflection behavior from effective plastic strain behavior of rebars due to arch action in stress transfer. From the simulation, showed approximately 95% similarity in average displacement at the design ultimate load (P_u) of 37.12 kN, and 94% similarity in average displacement at the ultimate load of 64 kN. The overall analysis results verified that the actual experiment and simulation values showed similar behavior.

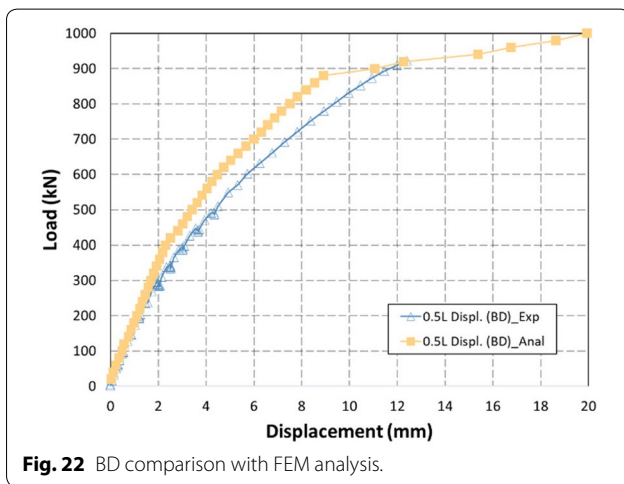
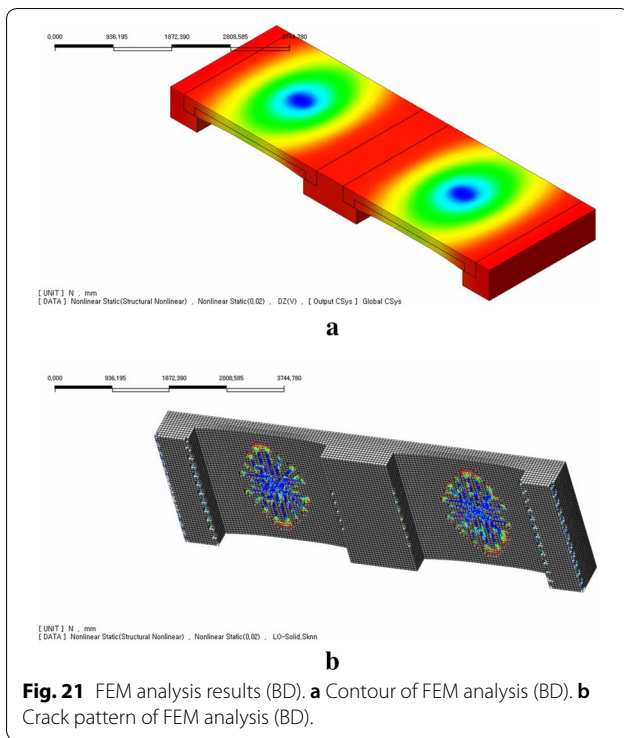


5.4 Analysis Results of BD Static Loading

The contour and crack pattern obtained from the finite element analysis results are shown in Fig. 21. The overall stress distribution showed a dispersed crack pattern in the longitudinal direction around the loading point. The reason for the longitudinal crack with radial shape than straight shape was due to the same as mentioned in the above experiment section.

Based on the analysis results, the load–displacement curve in Fig. 22 shows the comparison between the experiment and simulation results at the 1/2 position (0.5 L). MIDAS FEA was used for the simulation by applying the same boundary conditions and material properties to those used in the experiment. As depicted in the curve, similar behavior between test and simulation results were observed below loading of approximately 300 kN. However, the stiffness of the analysis result beyond 300 kN was slightly higher than the stiffness of the experimental results. In addition, starting from a load of 880 kN, the deflection of the specimen increased abnormally. This abnormality derives from various factors such as softening effect of rebars, cracking effect of concrete, etc. Thus, the maximum load shown in the simulation results was approximately 880 kN, which occurred prior to the softening action. This behavior of softening indicates that the member completely failed. This was approximately 95% level of the maximum load at 922.80 kN of the specimen. The reason for the difference between the experiment and simulation results was due to inevitable errors that can occur in tests, such as boundary conditions of the specimen and accurate loading conditions of the actuator. The above result differences between the test and simulation may be reduced if the average values from the three specimens to compare to the simulation results. Nonetheless, since the result differences was less than





approximately 5%, the simulation results can be considered accurate.

6 Conclusions

This study conducted flexural behavior experiments to verify the structural performance of the arch deck and 2-span arch deck composite specimen (BD), which is currently under development in Korea. The conclusions obtained through this experiment were as follows.

1. The experiment results of AD specimen, the maximum static loads of three specimens were 63.20, 61.10, and 69.15 kN, and the mean value was 64.48 kN. This is a level of approximately 1.6–1.9 times the design ultimate load (P_u) 37.12 kN. When applying this design load to the design of an actual structure, the safety factor is approximately 30% higher than the numerical design value. In BD specimen, the failure load of the BD was 922.80 kN, which is approximately 2.4 times the design ultimate load (P_u) of 384.31 kN, showing that the load carrying capacity of the arch deck was much higher than that of the design values obtained using a flat deck. In AD arch deck test results, the maximum failure load occurred at approximately 1.75 times the average design ultimate load. In BD arch deck test, the failure load occurred at approximately 2.4 times the design load due to better composite behavior between AD single deck and cast-in-place fill in overlay concrete.
2. The experiment results of AD specimen, since the yield strength of the rebar was 400 MPa, the rebar would yield when the strain rate exceeds approximately 0.002. However, the strain data showed that plastic strain occurred in the rebar at the 1/2 position after a strain of approximately 0.0026. The above results indicate that the yield strain increased due to the arch action from the arch shape of the deck and the combined with rebars and concrete. Due to these reasons, it is considered that strains of rebars, which was embedded in concrete were a little different from the original rebars. Also, the load reached a failure load of approximately 60 kN, while the concrete strain did not reach a concrete compressive strain limit of 0.003. This result indicated that compressive region of the specimens may have structural resistance even at a ultimate load from the experiment of 60 kN. In BD specimen, as analyzed in previous studies, plastic strain of the rebar actually occurred after total strain of approximately 0.0026, which is the same strain behavior shown in the AD test. For the above reason, the rebar yielded at approximately 900 kN and a total strain of 0.0026 rather than at approximately 750 kN and a total strain of 0.002 of the design value. Also, the maximum concrete strain occurred at the 1/2 position and was approximately 0.0017, which is less than the ultimate concrete compressive strain of 0.003. A compressive failure did not occur in the specimen even at the ultimate load of 922.80 kN, showing that the arch deck has sufficient resistance against brittle compressive failure.
3. The experiment results of AD specimen, the overall crack pattern of a longitudinal macro-cracks was observed at the center of the specimen. However, no

longitudinal and lateral cracks were observed beyond the 1/4 position, which once again shows that arch action occurred in the load transferring process where the macro-cracking occurred at the weakest location, the top of arch in the specimen. In BD specimen, the initial crack occurred at a load of approximately 250 kN. Since the design crack load (P_{cr}) was 128.62 kN, the actual crack load was approximately 1.9 times the design crack load, which verifies effective load transfer in the structure due to arch action. In CRB 1, the separation distance at the AD joints progressed rapidly at a load of approximately 300 kN, due to increasing overall displacement and strain. This is an inevitable result when using the precast deck construction, resulting in formation of multiple cracks. Also, since this joint cracking load was approximately 2.33 times higher than the design crack load (P_{cr}) of 300 kN, it is possible to disregard the cracks and consider them to be insignificant defect in structural performance.

- The simulation results of AD, showed approximately 95% similarity in average displacement at the design ultimate load (P_u) of 37.12 kN, and 94% similarity in average displacement at the ultimate load of 64 kN. The overall analysis results verified that the actual experiment and simulation values showed similar behavior. In BD simulation, the maximum load shown in the simulation results was set to approximately 880 kN, which was prior to the occurrence of the softening action. This was approximately 95% level of the maximum load at 922.80 kN of the specimen. The above result differences between the test and simulation may be reduced if the average values from the three specimens to compare to the simulation results. Nonetheless, since the result differences was less than approximately 5%, the simulation results can be considered accurate.

The summary of the above results demonstrated that the structural performance of AD and BD specimen was sufficiently stable and will have sufficient resistance performance even if it is used for long span deck.

Authors' contributions

D-HY: a person who performed most of test and analysis works; a main writer of the paper. M-JK: a person who assisted the research and writing the paper. G-HE: a person who assisted the research and writing the paper. J-HJK: a PI of the research project, who planned and developed the main idea of the study. All authors read and approved the final manuscript.

Acknowledgements

This research was supported by the Korea Agency for Infrastructure Technology Advancement funded by the Ministry of Land, Infrastructure and Transport of the Korean government (Project No.: 16TBIP-C111156-01).

Competing interests

The authors declare that they have no competing interests.

Availability of data and materials

Not applicable.

Publisher's Note

Springer Nature remains neutral with regard to jurisdictional claims in published maps and institutional affiliations.

Received: 5 March 2018 Accepted: 4 July 2018

Published online: 26 September 2018

References

- Bhawar, P. D., Wakchaure, M. R., & Nagare, P. N. (2015). Optimization of pre-stressed concrete girder. *International Journal of Research in Engineering and Technology (Ijret) Eissn*, 4, 2319–3163.
- Cheng, J. (2010). Optimum design of steel truss arch bridges using a hybrid genetic algorithm. *Journal of Constructional Steel Research*, 66(8–9), 1011–1017.
- Cho, J. R., Kim, D. S., Kim, Y. J., Kwark, J. W., & Jang, S. Y. (2013). Three dimensional model for dynamic moving load analysis of a PSC-I girder railway bridge. *Journal of the Korean Society for Railway*, 16(4), 286–297. **(in Korean)**.
- Choi, K. H., Park, B. C., Choi, S. W., & Ryu, D. H. (2017). A study on the structural performance of deck-column joint at flat plate structure using ECC. *Journal of the Korea Concrete Institute*, 29(2), 209–216. **(in Korean)**.
- Cury, A., & Cremona, C. (2010, January). Long term dynamic monitoring of a PSC box girder bridge. In IABSE Symposium Report (Vol. 97, No. 19, pp. 22–29). International Association for Bridge and Structural Engineering.
- Dey, T. K., Srivastava, I., Khandelwal, R. P., Sharma, U. K., & Chakrabarti, A. (2013). Optimum design of FRP rib core bridge deck. *Composites Part B Engineering*, 45(1), 930–938.
- Han, M. Y., Hwang, E. S., & Lee, C. (2003). Prestressed concrete girder with multi-stage prestressing concept. *ACI Structural Journal*, 100(6), 723–731.
- Han, M. Y., Jin, K. S., & Choi, S. H. (2010). Flexural test for a monolithic holed web prestressed concrete (HWPC) girder. *International Journal of Concrete Structures and Materials*, 4(2), 77–87.
- Han, M. Y., & Kim, B. H. (2001). A Study on the effect of design parameters on the girder depth of IPC girder continuous bridges. *Journal of The Korean Society of Civil Engineers*, 21(4), 535–546. **(in Korean)**.
- Heyman, J. (1982). *The Masonry Arch*. Chichester: Ellis Horwood Ltd.
- Hordijk, D. A. (1991). *Local Approach to Fatigue of Concrete*. Doctoral Dissertation, Delft University of Technology.
- Issa, M. A., Idriss, A. T., Kaspar, I. I., & Khayyat, S. Y. (1995). Full depth precast and precast, prestressed concrete bridge deck panels. *PCI Journal*, 40(1), 59–80.
- Jeon, S. J., Choi, M. S., & Kim, Y. J. (2011). Graphical assessment for span ranges of PSC girder bridges. *Journal of Bridge Engineering*, 17(2), 343–352.
- Jeong, J. P., & Kim, W. (2014). Shear resistant mechanism into base components: Beam action and arch action in shear-critical RC members. *International Journal of Concrete Structures and Materials*, 8(1), 1–14.
- Jung, D. S., & Kim, C. Y. (2013). Finite element model updating of a simply supported skewed PSC I-girder bridge using hybrid genetic algorithm. *KSCCE Journal of Civil Engineering*, 17(3), 518–529.
- Kim, W. J., Cho, K. S., Lee, C. D., Kim, C. S., An, K. U., & Choi, J. H. (2012). Gyopo Bridge: A Double-Tied Arch Bridge in Poseung–Pyeongtaek Railroad. *Structural Engineering International*, 22(1), 26–28.
- Kim, J., Chung, W., & Kim, J. H. J. (2008). Experimental investigation on behavior of a spliced PSC girder with precast box segments. *Engineering Structures*, 30(11), 3295–3304.
- Kim, Y. J., Chung, C. H., & Park, C. L. (1997). Application of precast concrete bridge decks for rapid construction. *Journal of the Korea Concrete Institute*, 9(1), 68–75. **(in Korean)**.
- Kim, H. Y., & Jeong, Y. J. (2009). Steel–concrete composite bridge deck slab with profiled sheeting. *Journal of Constructional Steel Research*, 65(8–9), 1751–1762.
- Kim, S. J., Kim, J. H. J., Yi, S. T., Noor, N. B. M., & Kim, S. C. (2016). Structural performance evaluation of a precast PSC curved girder bridge constructed

- using multi-tasking formwork. *International Journal of Concrete Structures and Materials*, 10(3), 1–17.
- Kim, S. H., Lee, C. G., Kim, S. J., & Won, J. H. (2011). Experimental study on joint of spliced steel—PSC hybrid girder, part II: full-scale test of spliced hybrid I-girder. *Engineering Structures*, 33(9), 2668–2682.
- King, R. (2010). *Brunelleschi's Dome: The story of the great cathedral in florence*. New York: Random House.
- Korea Institute of Bridge and Structural Engineering (KIBSE). (2015). *Korean Highway Bridge Design Code (Limit State Design) Commentary*. Seoul: Geonseoljeongbosa. **(in Korean)**.
- Korea Standard Association (KSA). (2016). *KS D 3504; steel bars for concrete reinforcement* (pp. 1–31). Seoul: Korea Standards Association. **(in Korean)**.
- Lho, B. C., & Cho, G. D. (2007). A Study on the composite behavior according to height change of lattice bar in LB-DECK. *Journal of the Korean Society of Civil Engineers*, 27(2A), 193–200.
- Ma, Y. S., Wang, Y. F., & Mao, Z. K. (2011). Creep effects on dynamic behavior of concrete filled steel tube arch bridge. *Structural Engineering & Mechanics*, 37(3), 321.
- Marefat, M. S., Ghahremani-Gargary, E., & Ataei, S. (2004). Load test of a plain concrete arch railway bridge of 20-m span. *Construction and Building Materials*, 18(9), 661–667.
- Matta, F., Nanni, A., Ringelstetter, T. E., & Bank, L. C. (2006). Rapid construction of concrete bridge deck using prefabricated FRP reinforcement. In CICE 2006, third international conference on FRP composites in civil engineering, 13–15.
- Nam, J. W., Kim, H. J., Yi, N. H., Kim, I. S., Kim, J. H. J., & Choi, H. J. (2009). Blast analysis of concrete arch structures for FRP retrofitting design. *Computers and Concrete*, 6(4), 305–318.
- Nazmy, A. S. (1997). Stability and load-carrying capacity of three-dimensional long-span steel arch bridges. *Computers & Structures*, 65(6), 857–868.
- Ryu, H. K., Chang, S. P., & Kim, Y. J. (2003). Experimental works on the flexural behavior of precast reinforced concrete decks with loop joints. *Journal of the Korean Society of Civil Engineers*, 23(3A), 479–486. **(in Korean)**.
- Saleem, M. A., Mirmiran, A., Xia, J., & Mackie, K. (2011). Ultra-high-performance concrete bridge deck reinforced with high-strength steel. *ACI Structural Journal*, 108(5), 601.
- Shim, C. S., Chung, C. H., Kim, I. K., & Kim, Y. J. (2010). Development and application of precast decks for composite bridges. *Structural Engineering International*, 20(2), 126–133.
- Stamnas, P. E., & Whittemore, M. D. (2005). All-precast substructure accelerates construction of prestressed concrete bridge in New Hampshire. *PCI Journal*, 50, 3.
- Staquet, S., Rigot, G., Detandt, H., & Espion, B. (2004). Innovative composite precast prestressed precambered U-shaped concrete deck for Belgium's high speed railway trains. *PCI Journal*, 49(6), 94–113.
- Taylor, S. E., & Mullin, B. (2006). Arching action in FRP reinforced concrete slabs. *Construction and Building Materials*, 20(1–2), 71–80.
- Taylor, S. E., Rankin, G. I. B., & Cleland, D. J. (2001). Arching action in high-strength concrete slabs. *Proceedings of the Institution of Civil Engineers-Structures and Buildings*, 146(4), 353–362.
- Tokuno, M., Saito, F., Takeshima, S., & Nakai, Y. (2005). *U.S. Patent No. 6,892,410*. Washington, DC: U.S. Patent and Trademark Office.
- Willis, R. (1848). *The architectural history of York cathedral*. London: Office of the Archaeological Institute.
- Won, Y. S. (2013). *U.S. Patent No. 8,544,129*. Washington, DC: U.S. Patent and Trademark Office.
- Wu, Q., Yoshimura, M., Takahashi, K., Nakamura, S., & Nakamura, T. (2006). Non-linear seismic properties of the Second Saikai Bridge: A concrete filled tubular (CFT) arch bridge. *Engineering Structures*, 28(2), 163–182.

Submit your manuscript to a SpringerOpen[®] journal and benefit from:

- Convenient online submission
- Rigorous peer review
- Open access: articles freely available online
- High visibility within the field
- Retaining the copyright to your article

Submit your next manuscript at ► springeropen.com
